Semnan University

Journal of Heat and Mass Transfer Research

Journal homepage: http://jhmtr.journals.semnan.ac.ir

Investigation of the thermo-hydraulic behavior of the fluid flow over a square ribbed channel

Ali Sarreshtedari[1,*], Alireza Zamani Aghaee[1]

[1]*Mechanical Engineering Departmen, University of Shahrood, Shahrood, Semnan, Iran*

PAPER INFO

History:
Received 28 January 2014
Received in revised form 3 May 2014
Accepted 9 June 2014

Keywords:
Turbulent flow
Ribbed channel
Heat transfer
Pressure drop
Thermal - enhancement.

A B S T R A C T

The thermo-hydraulic behavior of the air flow over a two dimensional ribbed channel was numerically investigated in various rib-width ratio configurations (B/H=0.5-1.75) at different Reynolds numbers, ranging from 6000 to 18000. The capability of different turbulence models, including standard k-ε, RNG k-ε, standard k-ω, and SST k-ω, in predicting the heat transfer rate was compared with the experimental results and it was showed that the k-ε turbulent models best adapt with the measured data. Four main parameters, namely, the Nusselt number, friction factor, skin friction factor, and the thermal enhancement factor were examined through the simulations. Results indicate that an increase in the Reynolds number caused the Nusselt number to increase and the friction factor to drop. It was found that the thermal enhancement factor augmented by an increase in the Reynolds number, and also, for a wider rib, i.e. at the higher the B/H ratio, a lower thermal enhancement factor was obtained.

1. Introduction

Investigating the heat transfer in turbulent flows over the surfaces of a wall mounted bluff bodies has significant importance in many engineering applications and is still a challenging problem in fluid mechanics. There is always a great deal of interest in accurately modeling the turbulent behavior of the fluid flow over rough surfaces [1, 2]. The most regularly used roughness elements are repeated winglets, grooves, and ribs which are mounted periodically along the inner walls of the pipes or channels to generate new turbulent regions within the core flow, hence they enhance the heat transfer. Another important application of the periodic surfaces mounted as obstacles is in heat exchanging industries to reduce the size, weight, and cost of the heat exchangers. To develop compact and highly efficient heat exchangers, the convective heat transfer coefficient should be raised in the inner tubes. One of the most efficient methods for increasing the convective heat transfer is introducing the artificial roughness on the inner tubes [3]. Interior roughness and vortex generating structures enhance the heat transfer by perturbing the flow in layers adjacent to the inner tube wall. However, this perturbation in the fluid flow would result in an increase in the pressure drop over the surface which may be undesirable. Therefore, great considerations should be taken in modeling and designing because of the twofold effects of such structures.

Lots of experimental studies have been presented on the heat transfer enhancement and pressure drop in ducts, annuli, and tubes with different kinds of roughen surfaces or turbulators. However, because of a wide variability of geometric parameters, a comprehensive investigation in this filed has been rarely found in literatures. Lai and Yang utilized the standard k–ε model and three low Reynolds number k–ε models to simulate the flow in a

Corresponding author: Ali Sarreshtedari, School of Mechanical Engineering, University of Shahrood, Shahrood, Semnan, Iran. *Email:sarreshtehdari@gmail.com*

pipe with a ring-shaped turbulator installed in the near-wall region [15]. Iacovides and Raisee [16] studied the convective heat transfer in the two-dimensional ribbed channels using low Reynolds number turbulence models. Kim et al. [17] studied the flow and thermal characteristics of a channel with surface mounted heat generating blocks for developing laminar flow. Meinders et al. [18] presented the results of the experimental investigation of the local convective heat transfer from a wall mounted single array of cubical protrusions along a wall of a wind tunnel at Re = 795, 2086, 3278 and 5066. Kahrom et al. [19] inserted a quad into a flat plate boundary layer and investigated its effect on the heat transfer rate and the friction factor. They also optimized the heat transfer enhancement by the use of multi objective genetic algorithm. Also to improve the heat transfer in a channel flow, Vatani and Mohammad [20] modeled the turbulent nanofluid flow over periodic rib-grooved channels.

In this paper, a periodic grooved channel with different groove-width ratio is modeled and heat transfer coefficient (Nu), friction factor (f) and the thermal enhancement factor are numerically investigated. Since the turbulence model is known to strongly affect the turbulent thermal characteristics, different turbulence models, including standard k−ε, Renormalized Group (RNG) k−ε, standard k−ω, and SST k−ω models, are applied and their abilities in the prediction are compared. A k−ε turbulence model is presented and its results are compared with other models. The effect of groove geometry on the heat transfer enhancement, pressure drop, and thermal enhancement is investigated for different values of groove-width ratio (B/H).

2. Mathematical Modeling

2-1 Flow field governing equations

The thermo-hydraulic behavior of the averaged fluid flow quantities is mathematically described by the continuity equation, Reynolds-averaged Navier-Stokes equations (RANS), and energy equation. The steady state form of these equations can be written in Cartesian framework as follows:

continuity equation:

$$\frac{\partial}{\partial x_i}(\rho u_i) = 0 \tag{1}$$

momentum equation:

$$\frac{\partial}{\partial x_j}(\rho u_i u_j) = -\frac{\partial P}{\partial x_i} + \frac{\partial}{\partial x_j}\left[\mu\left(\frac{\partial u_i}{\partial x_j} + \frac{\partial u_j}{\partial x_i}\right) - \rho\overline{u_i' u_j'}\right] \tag{2}$$

energy equation:

$$\frac{\partial}{\partial x_j}\left(\rho u_j T\right) = \frac{\partial}{\partial x_j}\left[(\Gamma + \Gamma_t)\frac{\partial T}{\partial x_j}\right] \tag{3}$$

where Γ and Γ_t are the molecular thermal diffusivity and turbulent thermal diffusivity, respectively given by"

$$\Gamma = \frac{\mu}{\Pr} \quad \text{and} \quad \Gamma_t = \frac{\mu_t}{Pr_t} \tag{4}$$

The term $-\rho\overline{u_i' u_j'}$ in eq.(2) is the Reynolds stress tensor which represents the mean flux of momentum due to the turbulent fluctuations, and should be modeled in RANS approaches.

2-2 Turbulence models

Many different turbulence models have been presented in order to model the Reynolds stress term in the Navier-Stokes equation. For instance, the k-ε and k-ω turbulence models, which are used in the current work simulations, are introduced here.

2-2-1 The k-ε model

The standard k-ε model was originally developed and validated for incompressible thin shear flows [4]. Based on the Boussinesq hypothesis, the Reynolds stresses term can be related to the men velocity gradients as follows:

$$-\rho\overline{u_i' u_j'} = \mu_t\left(\frac{\partial u_i}{\partial x_j} + \frac{\partial u_j}{\partial x_i}\right) - \frac{2}{3}\rho k\delta_{ij} \tag{5}$$

where μ_t is the turbulent viscosity and is defined by an appropriate turbulence model. One of the introduced expressions for computing the turbulent viscosity is:

$$\mu_t = \rho C_\mu \frac{k^2}{\varepsilon} \tag{6}$$

in which k and ε represent the turbulent kinetic energy (TKE) and its rate of dissipation, and defined by eqs. (7) and (8), respectively:

$$\frac{\partial(\rho k)}{\partial t} + \frac{\partial(\rho k u_i)}{\partial x_i} = \frac{\partial}{\partial x_i}\left[\left(\frac{\mu_T}{\sigma_k} + \mu\right)\frac{\partial k}{\partial x_i}\right] + \mu_T\left[S - \frac{2}{3}\left(\frac{\partial u_l}{\partial x_l}\right)^2\right] - \frac{2}{3}\rho k\frac{\partial u_i}{\partial x_i} - \rho\varepsilon \tag{7}$$

$$\frac{\partial(\rho\varepsilon)}{\partial t} + \frac{\partial(\rho\varepsilon u_i)}{\partial x_i} = \frac{\partial}{\partial x_i}\left[\left(\frac{\mu_T}{\sigma_\varepsilon} + \mu\right)\frac{\partial \varepsilon}{\partial x_i}\right] + \mu_T C_1\frac{\varepsilon}{k}\left[S - \frac{2}{3}\left(\frac{\partial u_l}{\partial x_l}\right)^2\right] - \frac{2}{3}C_1\rho\varepsilon\frac{\partial u_i}{\partial x_i} - C_2\rho\frac{\varepsilon^2}{k} + C_3\rho\varepsilon\frac{\partial u_i}{\partial x_i} \tag{8}$$

where

$$S = \frac{1}{2}\left(\frac{\partial u_i}{\partial x_j} + \frac{\partial u_j}{\partial x_i}\right)^2 \tag{9}$$

The empirical constants of the standard k-ε model are C_1=1.44, C_2=1.92, C_3=-0.33, C_μ=0.09, Pr_t=0.9, σ_k=1 and σ_ε=1.3 [6].

The RNG (Renormalization Group) k-ε model is a modified form of the standard k-ε model which is first introduced by Yakhot and Orszag [7] to solve the incompressible flows. The k equation is the same as the standard k-ε model, eq.(7) , but the ε equation is modified to:

$$\frac{\partial(\rho\varepsilon)}{\partial t} + \frac{\partial(\rho\varepsilon u_i)}{\partial x_i} = \frac{\partial}{\partial x_i}\left[\left(\frac{\mu_T}{\sigma_\varepsilon} + \mu\right)\frac{\partial \varepsilon}{\partial x_i}\right] \tag{10}$$

$$+\mu_T C_1 \frac{\varepsilon}{k}\left[S-\frac{2}{3}\left(\frac{\partial u_l}{\partial x_l}\right)^2\right]-\frac{2}{3}C_1\rho\varepsilon\frac{\partial u_i}{\partial x_i}-C_2\rho\frac{\varepsilon^2}{k}$$
$$+C_3\rho\varepsilon\frac{\partial u_i}{\partial x_i}-\rho\frac{\vartheta_T S^3(1-\eta/\eta_0)}{1+\beta\eta^3}$$

where η is the turbulent to the mean strain-time scale ratio ($\eta = S\frac{\bar{k}}{\bar{\varepsilon}}$), η_0 is its initial value and β is a constant. The standard constants of the RNG k-ε model are C_1=1.42, C_2=1.92, C_3=-0.33, C_μ=0.09, σ_k=1 and σ_ε=0.719.

2-2-2 The k-ω model

k- ω is another two-equation turbulence model which uses the concept of the dissipation rate of energy per unit volume, and per time and is related to the external scale of turbulence, *l*, by:

$$\omega = \frac{ck^{0.5}}{l} \qquad (c\ is\ a\ constant) \tag{11}$$

The k-ω transport equations are [9]:

$$\frac{\partial}{\partial x_i}\left(\rho u_i k-\rho(\vartheta+\sigma^*\vartheta_T)\frac{\partial k}{\partial x_i}\right)=\tau_{ij}\frac{\partial u_i}{\partial x_j}-\beta^* k\omega \tag{12}$$

$$\frac{\partial}{\partial x_i}\left(\rho u_i \omega-\rho(\vartheta+\sigma\vartheta_T)\frac{\partial \omega}{\partial x_i}\right)=\alpha\frac{\omega}{k}\tau_{ij}\frac{\partial u_i}{\partial x_j}-\beta\omega^2 \tag{13}$$

where the detailed description of the parameters appeared in the above equations can be found in the reference [10].

3. Numerical Method

3-1 geometry and computational grid

The experimental setup of Lorenz et al. [11] is used here for numerical simulations. The system is a two dimensional [12] ribbed horizontal plane channel, whose configuration is illustrated in fig. (1) and table (1). The lower wall of the channel is equipped with eight ribs which make the test section of the current case. The heat flux of the test section is provided by a constant electrical heat flux, while the upper wall of the channel is kept adiabatic. In order to maintain the fully developed condition, the ribbed test section is located 20H downstream of the entrance and 10H upstream of the exit. For studying the effect of the ribbed surface geometry on the flow behavior, different rib-width ratios, B/H=0.5, 0.75, 1, 1.25, 1.5 and 1.75, are modeled here.

Table 1. The ribbed channel configuration

configuration	dimension
Channel height, H (constant in all cases)	40 mm
Test section length, L	17H
Rib height, e	0.5H
Rib length, S	H
Groove width, B	0.5H, 0.75H, H, 1.25H, 1.5H, 1.75H

Upper and lower walls and ribs walls are set to fixed walls while inlet flow and outlet flow conditions are adjusted with constant velocity and constant pressure conditions, respectively.

To resolve the rapidly changing flow structures, to reach efficient numerical solution, and to save the computational time, a uniform rectangular mesh with grid adoption for $y^+\approx2$ at an adjacent wall region is used, while a fine mesh is generated close to the walls and ribs, fig. (2). Generation of the computational grid is done by the GAMBIT 2.3.16 software. Grid independence study was carried out to reduce the uncertainties associated with mesh. Calculations shows that grid independent results can be obtained for standard turbulence models with 2.5×10^6 elements.

3-2 Solution procedure

The commercial CFD software FLUENT 6.3.26 is used to solve equations numerically. The second order upwind differentiating scheme is applied to the convective and turbulent terms, and also the energy equation. The diffusion terms are discretized by the second order central differencing scheme. To evaluate the pressure field, SIMPLE (Semi Implicit Method for Pressure Linked Equation) algorithm is used for coupling the pressure and velocity terms [13]. The boundary conditions applied is tabulated in table (3). The average Nusselt number is the dimensionless parameter used for assessing the heat transfer enhancement and is defined as:

$$Nu = \frac{1}{L}\int\frac{h(x).D_h}{k}dx \tag{14}$$

where h(x) is the convective heat transfer coefficient and is estimated in any position, related to flow condition and fluid properties. k is the thermal conductivity. D_h is the hydraulic diameter of the channel and is equal to 2H [11]. The friction factor, f, and the skin friction coefficient, C_f, are the parameters used for the pressure drop evaluation along the channel. The friction factor over a test section of length L with a pressure drop of ΔP is calculated by:

$$f = \frac{\Delta P.D_h}{\frac{1}{2}\rho u^2 L} \tag{15}$$

The skin friction factor given by eq. (15) is related to the wall shear stress:

$$C_f = \frac{\tau_w}{\frac{1}{2}\rho u^2} \tag{16}$$

In order to investigate the dual effect of turbulence on thermo-hydraulic behavior of the flow, namely enhancing the heat transfer and increasing the pressure drop, the thermal enhancement factor is introduced as [14]:

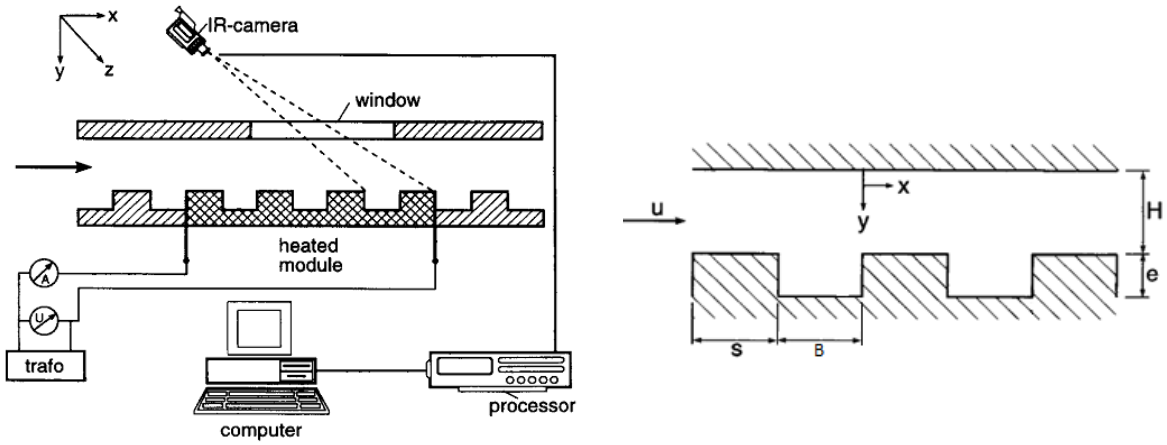

Fig.1 The geometry of the case under consideration [11]

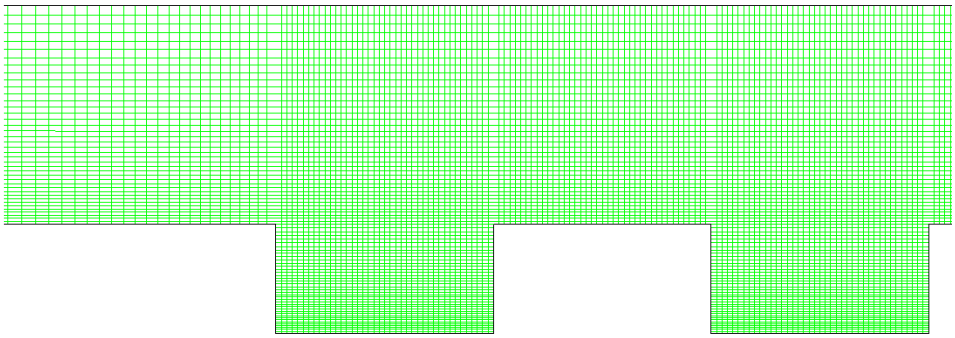

Fig.1 computational grid

$$\eta = \frac{(Nu/Nu_s)}{(f/f_s)^{1/3}} \quad (17)$$

where subscript s represents the smooth channel properties.

4. Results and Discussion

The capability of different turbulent models in predicting the average Nusselt number variation over a single rib is shown in fig. (3) and the results are compared with the experimental results [11]. The results are plotted for the case of B/H=1 and Re=12000. As it can be seen, Nu is decreased up to ξ/H=2 because of the boundary layer growth, and then the recirculation zone is generated due to the turbulence causes the Nu increase. It is also found that the maximum average Nusselt number over a single rib occurs at the front edge of the rib's top surface (B/H=0.5), where the shear layer reattaches. From this stagnation point, the flow bifurcates into the main flow through the clear channel and into the recirculation flow in the groove. This bifurcation yields two thermal boundary layers along the top of the rib ($0.5 < \xi/H < 1.5$) and along the front flank that cause high local and global heat transfer rates on the grooved wall. The Nusselt number distribution along the top of the rib is almost parallel to that of a thermally developing boundary layer, except for a relatively stronger decrease near the rear edge of the rib ($1.45 < \xi < 1.5$). Along the front flank, the Nusselt number decreases almost linearly from the stagnation point. At the bottom of the groove and near the corner formed with the front flank of the rib ($\xi/H \approx 3$), the Nusselt number distribution has a local minimum. This can be interpreted as the effect of a secondary vortex in the corner at $\xi/H = 3.0$ and $\xi/H = 0$, respectively. At the opposite bottom corner ($\xi/H = 2.0$) and near the rear flank, no similar effect is visible.

Comparing the abilities of different turbulent models in predicting the Nu yields that the k-ε models show a better agreement with the experimental results especially in the grooved zone, where the turbulence and vortexes/recirculation zone exist. The error analysis of the comparison with the experimental results illustrates that there exists less than 10% variation for k-ε models

Table 2. Boundary condition

fluid	Air at standard atmospheric condition
inlet	Uniform velocity (based on the Reynolds number ranged from 6000 to 18000)
outlet	Constant pressure
Upper wall	Adiabatic wall
Lower wall	Constant heat flux at the test section No slip

while more differences may be observed for k-ω models (up to 27%). Hence, either the standard k-ε model or RNG k-ε model can be used for investigating the thermo-hydraulic behavior of the fluid flow. In the present paper, the RNG k-ε turbulent model is applied to the simulations.

The velocity vectors in the grooved zone are plotted in fig. (4). The recirculation domain is predicted to have a larger area in the standard k-ε model compared with the k-ω models, while k-ω models best show the second vortex domain produced at the beginning of the grooved surface.

The flow structure over the ribbed surface of different geometries is shown in fig. (5) using the stream function contours. As it can be seen, a higher B/H, i.e. a larger groove, obtains a bigger recirculation zone.

To verify thermal periodicity [Nu(ξ) = Nu(ξ+Period)], the local Nusselt number distributions on the top surface of all ribs ($0.5 \leqslant l/H \leqslant 1.5$) are presented in fig. 7. Numerical results show that the periodical thermal condition is reached after the fifth period at any Reynolds number.

The variation of the average Nusselt number over the test section is displayed in fig. (8). It is evident that Nu decreases until reaching the upstream of the test section.

Variation of the Nusselt number with respect to the Reynolds number is plotted for different width ratio geometries and is compared with the smooth channel case in fig. (9). As it is shown in the figure, an increase in the Reynolds number, and consequently the turbulence, results in an increase in the heat transfer rate. It is also found that the Nusselt number in all cases is much higher than the smooth channel case because the ribbed surface acts as a turbulator by inducing the high recirculation zone and by thinning the boundary layer. Furthermore, it is understood from this figure that the wider the groove, the higher the Nusselt number would be.

The friction factor is shown versus the Reynolds number for different ribbed geometries and is compared with the smooth case. Increasing the Reynolds number makes the viscous sub-layer suppressed which results in a decrease in the friction factor. Wider grooves also result in higher friction factor.

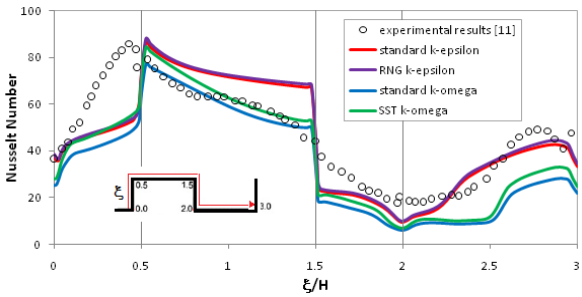

Fig.4 Capability of different turbulent models in predicting the Nu (B/H=1 and Re=12000)

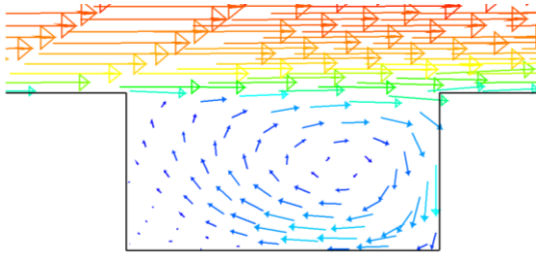

a) standard k-ε model

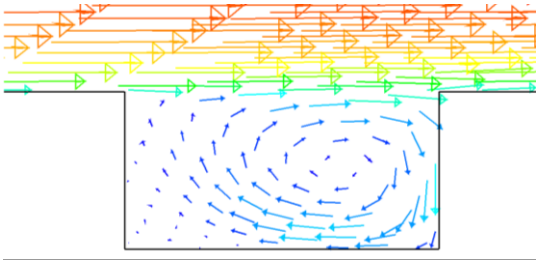

b) RNG k--ε model

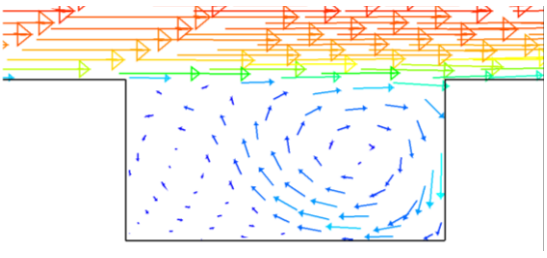

c) standard k-ω model

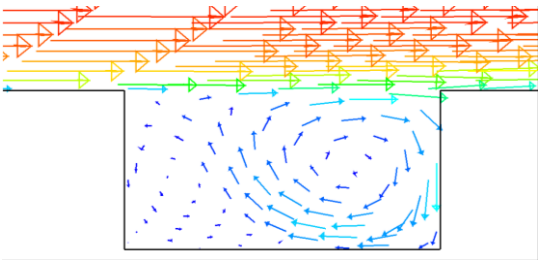

d) SST k-ω model

Fig.3 Capability of different turbulent models in showing the velocity vectors within a turbulent field

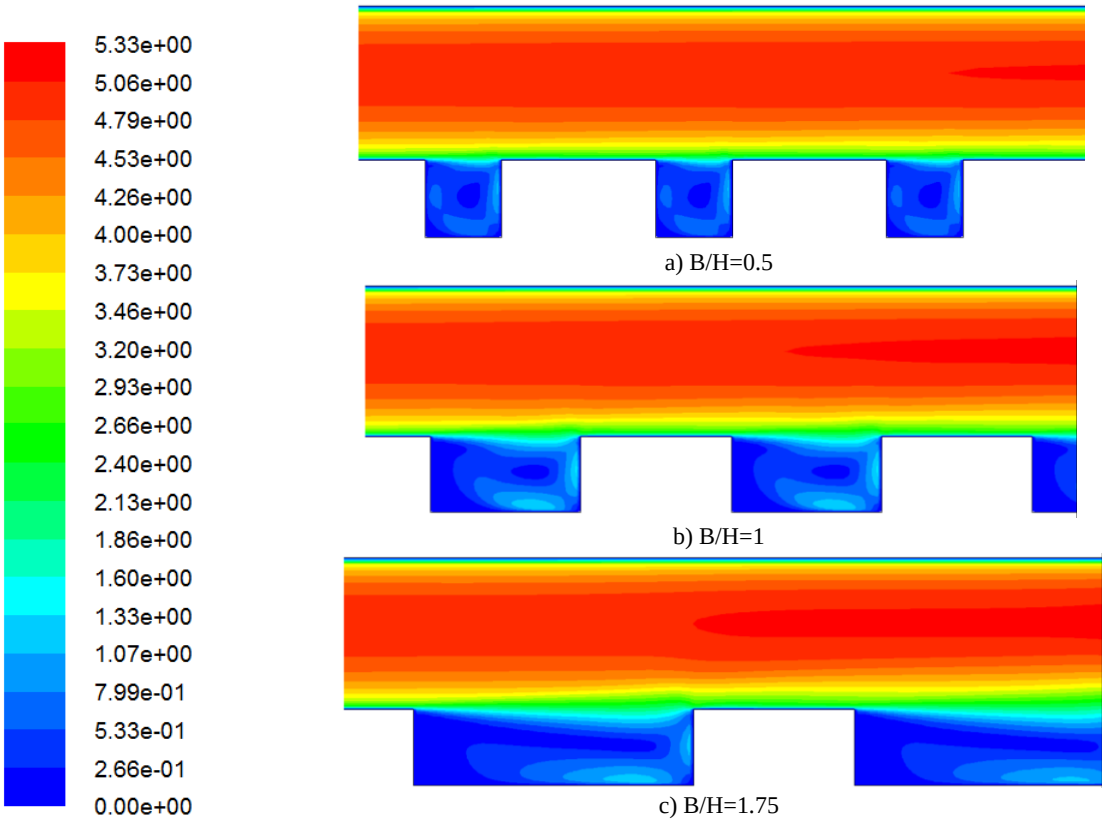

a) B/H=0.5

b) B/H=1

c) B/H=1.75

Fig.2 The stream function (velocity contour (m/s)) at the 8th rib zone

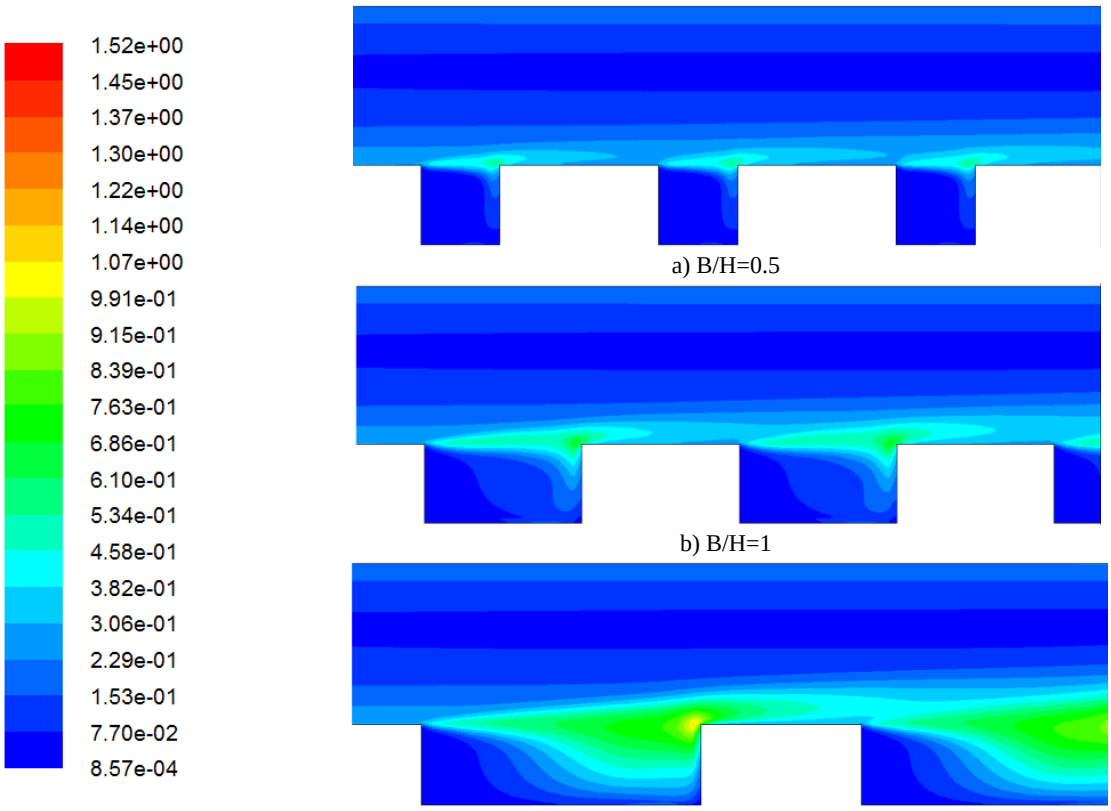

a) B/H=0.5

b) B/H=1

c) B/H=1.75

Fig.3 The turbulent kinetic energy contour at the 8th rib zone

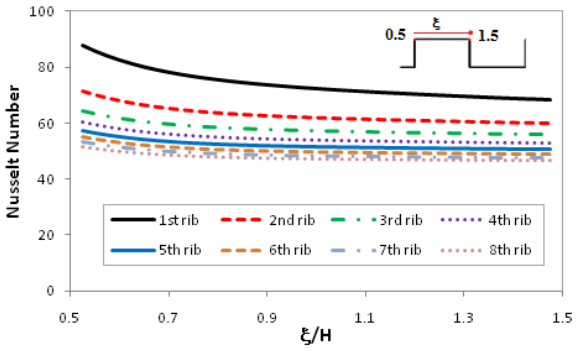

Fig.4 Nusselt number distribution over the rib surface

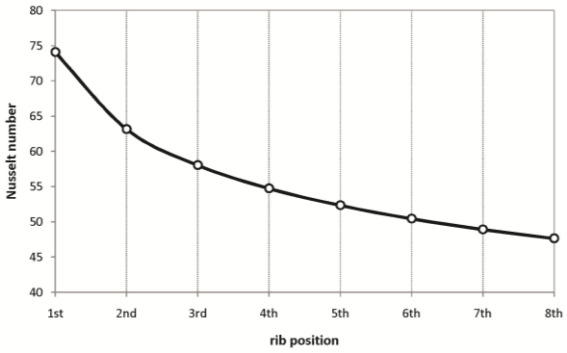

Fig.5 Nusselt number distribution over the ribbed test section

Fig. (11) presents the distribution of the local skin friction coefficient over the last rib. The skin friction factor variation is interpreted the same as the Nusselt number variation over the rib. The maximum occurs at the frontal area of the rib's top surface and reaches its minimum value at the bottom surface of the groove.

As mentioned previously the turbulence has two different effects on the thermo-hydraulic behavior of the flow, namely, increasing the heat transfer rate and increasing the pressure drop. This fact is demonstrated in fig. (12) by comparing the amount of Nusselt number and friction factor of the grooved channel with the smooth one at different Reynolds numbers.

Thermal enhancement factor is shown in fig. (13). It is recognized that increasing the Reynolds number causes the thermal enhancement factor to increase. It is also found that lower B/H ratios yield higher thermal enhancement factors.

Other thermo-hydraulic parameters which can be studied, especially in heat exchangers, are the temperature difference and the pressure drop which takes place over system. Fig. (14) displays the variation of these items along the whole channel length. As expected, the temperature and the pressure drop show the same trend as the Nusselt number and the friction factor, shown in fig. (12), respectively.

In order to simultaneously assess the opposite twofold effects of turbulence on the behavior of the flow, the

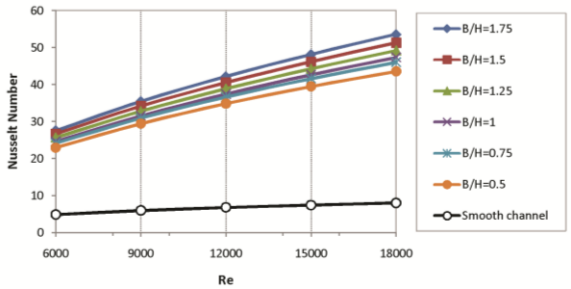

Fig.6 Nusselt number variation vs Reynolds number for different geometries

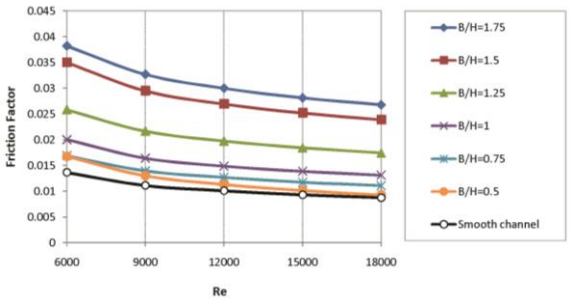

Fig.7 Friction factor variation vs Reynolds number for different geometries

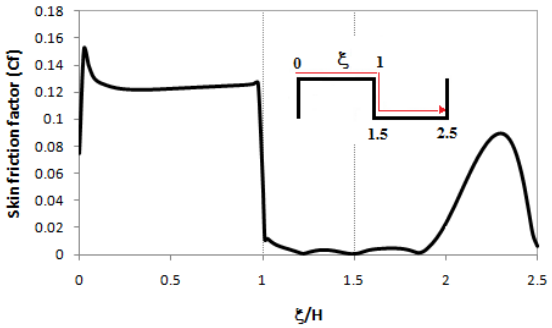

Fig.8 Skin friction factor distribution over the last pitch (8th rib)

ratio of these two parameters is plotted in fig. (15). It is seen that the maximum amount of temperature increment and the minimum amount of pressure drop occur at 0.75< B/H<1.

5. Conclusion

The heat transfer enhancement and the pressure drop are numerically investigated in the present study. Comparing the Nusselt numbers obtained from different turbulent models reveals that the k-ε turbulent models are qualitatively best agreed with the experimental results. The results showed that the thermal periodic condition is achieved after the fifth rib. The stagnation point occurring at the frontal area of the rib's top surface yields

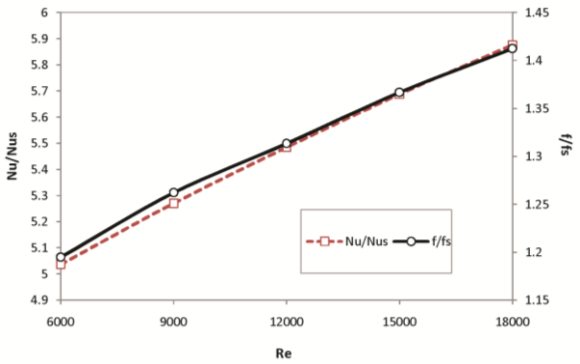

Fig.9 Variation of Nusselt number and friction factor with respect to the smooth channel case at different Reynolds number

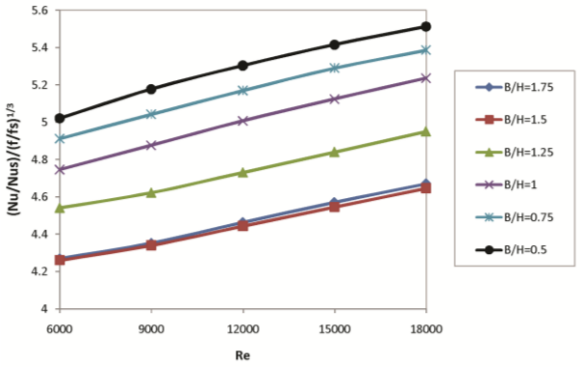

Fig.10 Thermal enhancement variation vs Reynolds number for different geometries

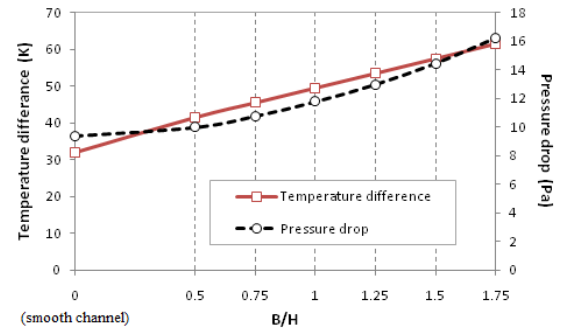

Fig.11 Temperature increase and pressure drop variations vs rib-width ratio

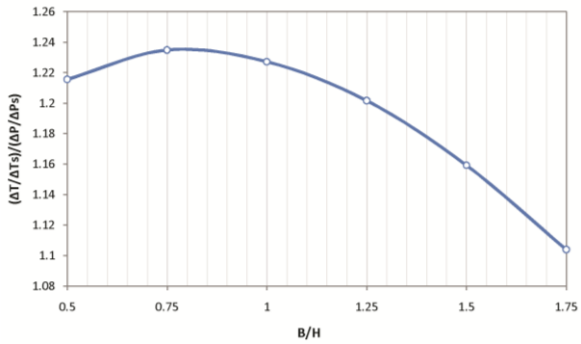

Fig.12 Thermal efficiency variation with rib width ratio

the maximum amount of heat transfer rate and also the skin friction factor, while these parameters reach their minimum values at the rear flank. Results indicate that an increase in the Reynolds number caused the Nusselt number to increase and the friction factor to drop. It is also found that the thermal enhancement factor shows an increasing trend with respect to increasing Reynolds number and decreasing B/H ratio.

Acknowledgment

The authors are very grateful to Dr. Mohammad Javadi and Mr. Mohammad Erfanian for their helpful discussions.

References

[1]. J.M. Robertson, J.D. Martin and T.H. Burkhurt, Turbulent flow in rough pipes, Ind. Eng. Chem. Fundam. 7, pp. 253–265, (1963).
[2]. J. Jiménz, Turbulent flow over rough walls, Annu. Rev. Fluid Mech. 36, pp. 173–196, (2004).
[3]. R.L. Webb, Principles of enhanced heat transfer, New York: Wiley, (1994).
[4]. W.P. Jones and B.E. Launders, The Prediction of Laminarization with a Two-Equation Model of Turbulence, Int. J. Heat Mass Transfer, Vol. 15, pp. 301-314, (1972).
[5]. A.D. Gosman and A.P. Watkins, A Computer Prediction Method for Turbulent Flow and Heat Transfer in Piston/Cylinder Assemblies, Proc. of a Symposium on Turbulent Shear Flow, (1977).
[6]. B.E. Launder and D.B. Spalding, Lectures in Mathematical Models of Turbulence, Academic Press, London, (1972).
[7]. V. Yakhot and S.A. Orszag, Renormalization Group Analysis of Turbulence, I. Basic Theory, J. Sci. Comput., Vol. 1, pp. 3-51, (1986).
[8]. W. Rodi, Turbulence Models and Their Application in Hydraulics - A State of the Art Review, IAHR, Netherlands, (1984).
[9]. DC. Wilcox, Turbulence modeling for CFD, California, USA: DCW Industries, Inc., (2000).
[10]. P. Zamankhan, Heat transfer in counterflow heat exchangers with helical turbulators, Commun Nonlinear Sci Numer Simulat, Vol. 15, pp. 2894-2907, (2010).
[11]. S. Lorenz, D. Mukomilow and W. Leiner, Distribution of the heat transfer coefficient in a channel with periodic transverse grooves, Experimental Thermal and Fluid Science, Vol. 11, pp. 234–242, (1995).
[12]. A. Chaube, P.K. Sahoo and S.C. Solanki, Analysis of heat transfer augmentation and flow characteristics due to rib roughness over absorber plate of a solar air heater, Renewable Energy, Vol. 31, pp. 317–331, (2006).
[13]. S.V. Pantankar, Numerical heat transfer and fluid flow. New York: Hemisphere, (1980).
[14]. C. Thianpong M. Pimsarn and P. Promvonge, Laminar periodic flow and heat transfer in tube with 45° angled ribs, Chiangmai University International Conference 2011, Vol. 1, No. 1 pp. 93-101, (2010).
[15]. J.C.S. Lai and C.Y. Yang, Numerical simulation of turbulence suppression: comparison of the performance of four k–e turbulence models, Int. J. Heat Fluid Flow, Vol. 18, pp. 578–584, (1997).
[16]. H. Iacovides and M. Raisee, Computation of flow and heat transfer in two-dimensional rib-roughened passages using low-Reynolds-number turbulence models, Int. J. Numer. Methods Heat Fluid Flow, Vol. 11, No. 2, pp. 138–155, (2001).

[17]. S.H. Kim and N.K. Anand, Laminar developing flow and heat transfer between a series of parallel plates with surface mounted discrete heat sources, Int. J. Heat Mass Transfer, Vol. 37, No. 15, pp. 2231–2244, (1994).

[18]. E.R. Meinders, K. Hanjalic and R. Martinuzzi, Experimental study of the local convective heat transfer from a wall mounted cube in turbulent channel flow, Trans ASME J. Heat Transfer, Vol. 121, pp. 564–573, (1991).

[19]. M. Kahrom, S.M. Javadi and P. Haghparast, Application of multi objective genetic algorithm to optimize heat transfer enhancement from a flat plate, international review of mechanical engineering, Vol. 4, No. 2, pp. 167-176, (2010).

[20]. A. Vatani, H.A. Mohammad, Turbulent nanofluid flow over periodic rib-grooved channels, Engineering Applications of Computational Fluid Mechanics, 7 (3), 369-381 (2013).